

Computational and biophysical approaches to protein–protein interaction inhibition of *Plasmodium falciparum* AMA1/RON2 complex

Emilie Pihan^{1,5} · Roberto F. Delgadillo¹ · Michelle L. Tonkin³ · Martine Pugnère⁴ · Maryse Lebrun² · Martin J. Boulanger³ · Dominique Douguet¹

Received: 5 November 2014 / Accepted: 25 March 2015 / Published online: 31 March 2015
© Springer International Publishing Switzerland 2015

Abstract Invasion of the red blood cell by *Plasmodium falciparum* parasites requires formation of an electron dense circumferential ring called the Moving Junction (MJ). The MJ is anchored by a high affinity complex of two parasite proteins: Apical Membrane Antigen 1 (*Pf*AMA1) displayed on the surface of the parasite and Rhoptry Neck Protein 2 that is discharged from the parasite and imbedded in the membrane of the host cell. Structural studies of *Pf*AMA1 revealed a conserved hydrophobic groove localized to the apical surface that coordinates RON2 and invasion inhibitory peptides. In the present work, we employed computational and biophysical methods to identify competitive *P. falciparum* AMA1–RON2 inhibitors with the goal of exploring the ‘druggability’ of this attractive

antimalarial target. A virtual screen followed by molecular docking with the *Pf*AMA1 crystal structure was performed using an eight million compound collection that included commercial molecules, the ChEMBL malaria library and approved drugs. The consensus approach resulted in the selection of inhibitor candidates. We also developed a fluorescence anisotropy assay using a modified inhibitory peptide to experimentally validate the ability of the selected compounds to inhibit the AMA1–RON2 interaction. Among those, we identified one compound that displayed significant inhibition. This study offers interesting clues to improve the throughput and reliability of screening for new drug leads.

Keywords Apicomplexa parasites · Malaria · Invasion · *Plasmodium falciparum* AMA1–RON2 interaction · Virtual screening · Fluorescence anisotropy based assay

Electronic supplementary material The online version of this article (doi:10.1007/s10822-015-9842-7) contains supplementary material, which is available to authorized users.

✉ Dominique Douguet
douguet@ipmc.cnrs.fr

¹ Institut de Pharmacologie Moléculaire et Cellulaire, Université de Nice Sophia-Antipolis, CNRS, UMR 7275, 660, Route des Lucioles, Sophia Antipolis, 06560 Valbonne, France

² UMR 5235 CNRS, Université de Montpellier 1 et 2, 34095 Montpellier, France

³ Department of Biochemistry & Microbiology, University of Victoria, PO Box 3055 STN CSC, Victoria, BC V8W 3P6, Canada

⁴ IRCM, Institut de Recherche en Cancérologie de Montpellier, INSERM U896, Université de Montpellier 1, ICM, Plateau de Protéomique Imagerie et Interactions Moléculaires, 34298 Montpellier, France

⁵ Present Address: ICOA, UMR7311, Université d’Orléans, Rue de Chartres, 45067 Orléans Cedex 2, France

Introduction

The phylum Apicomplexa includes some of the most important pathogenic parasites of man and animals, the deadliest of which is the malaria parasite *Plasmodium falciparum*, responsible for approximately 627,000 human deaths in 2012 [1]. Despite continuous efforts in vaccine development, prevention of malaria remains difficult, and the spread of drug-resistant parasites highlights the critical need for new antimalarial strategies [2].

Apicomplexa parasites have developed a unique invasion mechanism involving a tight interaction formed between the host cell and the parasite surface membranes called the Moving Junction (MJ) [3]. The MJ plays a central role in invasion as it anchors the parasite to the host surface while the parasite’s actin–myosin motor is

proposed to provide forward motion into the host cell [4, 5]. Formation of the MJ is initiated by injection of the Rhoptry Neck (RON) complex into the host cell, where RON2 spans the membrane and functions as a receptor for Apical Membrane Antigen 1 (AMA1) displayed on the parasite surface [6, 7]. Recently, the topology of RON2 at the host cell membrane has been determined and the region of RON2 that binds to AMA1 has been identified [8, 9]. Furthermore, it has been shown that peptides derived from this region of *Pf*RON2 (*Pf*RON2sp) are able to compete in the nanomolar range with the native *Pf*RON2 for *Pf*AMA1 interaction in vivo [8–10]. Since both AMA1 and RON2 are highly conserved, specific to Apicomplexa, and crucial for invasion [11, 12], interruption of the AMA1–RON2 interaction represents a potential intervention point for the development of anti-infective agents [13–19]. *Pf*AMA1 is also a major target of anti-malarial vaccine development [20] and AMA1 subunit vaccines may be highly effective when presented to the immune system as an invasion complex with RON2 [21]. The tractability of the *Pf*AMA1–RON2 complex for pharmacological intervention as also recently been investigated. Srinivasan et al. [22] used an HTS assay to screen a library of 21,733 compounds leading to the discovery of one small size inhibitor (NCGC00015280) of molecular weight of 370 with inhibitory effect in the micromolar range. Soon afterwards, however, a thorough binding analysis of this family of molecules by NMR suggested weaker binding affinities and unfavorable properties for further development [23]. Ge et al. [24] conducted a fragment-based screening campaign and identified competitive inhibitors of R1 peptide but their precise binding mode remains unclear making optimization difficult. More recently, Alam [25] reported a virtual screening of peptidomimetics but without experimental assessment. These studies highlight the importance of structural insight and experimental validation to the design of novel AMA1–RON2 inhibitors.

Protein–protein interactions (PPIs) play crucial roles in most cellular processes and represent an important type of targets for drug development with now some emerging success stories [26–29]. Additionally, with the benefit of hindsight resulting from experiences on enzyme inhibitors, it is acknowledged that drugs that mimic interactions of the endogenous ligand may improve affinity of weak hits [30] and, even overcome resistance mutations [31]. Ideally, tractable targets are transient ones possessing hotspots localized to a groove or pre-existing cavity that can accommodate a drug-sized molecule [32]. Structural studies of AMA1 revealed stacked three-domain architecture (DI, DII and DIII) with a conserved hydrophobic groove localized to the apical surface of DI that can accommodate a loop extending from domain II, called the DII loop [16, 33–39]. The co-structure of *Pf*AMA1 in complex with the *Pf*RON2sp1

peptide [2021–2059] is characterized by an extensive buried surface area of 1700 Å² and significant shape complementarity [17]. In addition, by extensive mutagenesis in both *Pf*RON2 and *Pf*AMA1, ‘hotspots’ have defined key residues governing the interactions between *Pf*AMA1 and *Pf*RON2 [17]. Key interactions are also supported by the co-structure of *Pf*AMA1 with the invasion-inhibitory peptide R1, a peptide screened by phage display that inhibits invasion [13–15, 17, 40, 41]. It is now acknowledged that using hotspots as the starting point for ligand identification is an efficient strategy when targeting PPIs [42, 43]. Since peptide-based therapeutics are difficult to develop, alternative compounds can be designed or identified through peptidomimetic approaches. In this study, we applied both ligand-based similarity and structure-based docking approaches to identify potential small molecule inhibitors of AMA1–RON2 interaction. To experimentally validate hits, we developed and optimized a fluorescence anisotropy (FA) assay [44] with a fluorescein labeled peptide, called F*R1-13A1, that binds *Pf*AMA1 at the same pocket as does native *Pf*RON2. Using these combined approaches, nine compounds were identified based on their pharmacophore and docking scores and were experimentally tested, and one molecule was found to have an IC₅₀ of 24 μM.

Materials and methods

Screening collection preparation

The structure of compounds from eight sources were prepared individually in 3D SDF format for virtual screening: (Ambinter (<http://www.ambinter.com/>), DrugBank (<http://www.drugbank.ca/downloads>), Chuprina’s library (referred as DL for ‘Drug Like’) [45], ChemBridge’s CombiLib and EXPRESS-Pick (<http://www.chembridge.com>), ChEMBL Malaria compounds (<https://www.ebi.ac.uk/chemblntd/download>) including the Malaria Box (<http://www.mmv.org/malariabox>), Chimiothèque Nationale (<http://chimiotheque-nationale.enscm.fr>) and e-Drug3D (<http://chemoinfo.ipmc.cnrs.fr/MOLDB/index.html>) [46]. Each structure was processed using Filter and Flipper programs to filter out inorganic 2D SDF structures and generate stereoisomers when necessary, respectively (OMEGA version 2.4.3., OpenEye Scientific Software, Santa Fe, NM., <http://www.eyesopen.com>). Molecules were then converted from 2D SDF to 3D SDF using the program Omega2 [47]. The most probable protonated and tautomeric forms at pH 7.4 were generated by the program QuacPac: tautomers (OpenEye Scientific Software, Santa Fe, NM., <http://www.eyesopen.com>). Finally, Omega2 was used to enumerate accessible conformations and Corina (Molecular Networks GmbH, <http://www.molecular-networks.com/>)

was used to generate ring conformations [48]. Conformers are essential when collections are filtered by rigid 3D-pharmacophore search programs. This processing resulted in 203,738,892 three-dimensional structures.

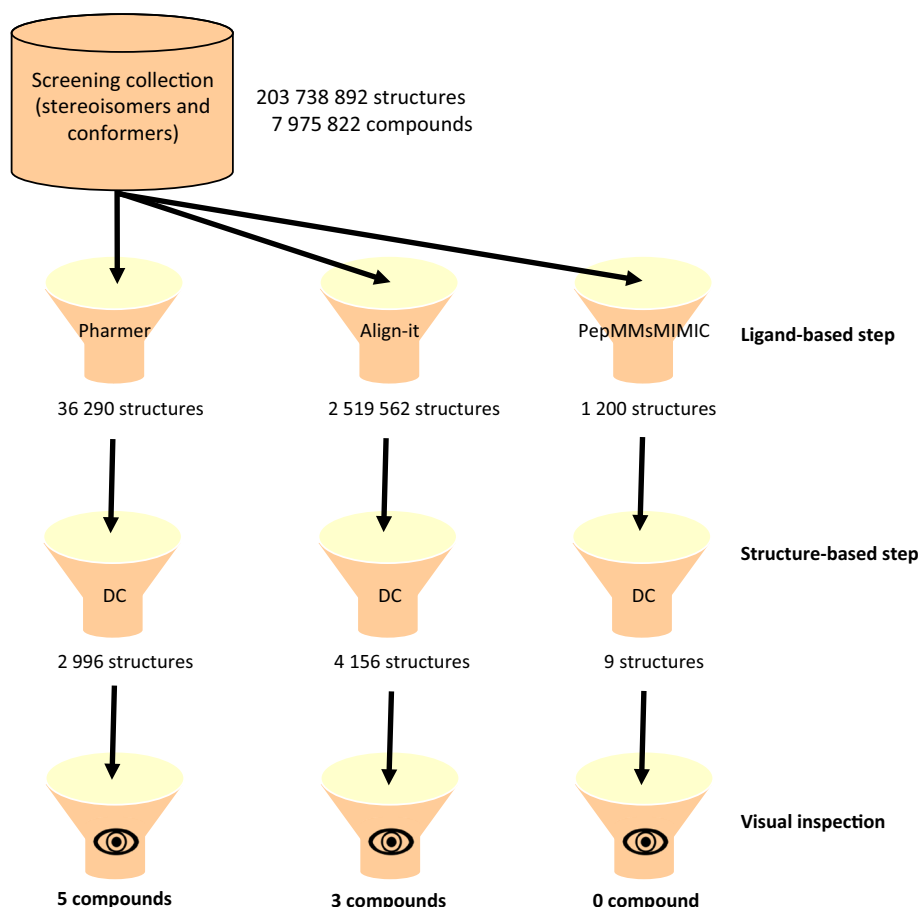
Virtual screening process (Fig. 1)

Ligand-based screens as initial filters

A pharmacophore model was generated using three different programs: (a) In Align-it (version 1.1.0; [49]; <http://silicos-it.com>), screens were performed by using the combination of the three-point pharmacophore model as well as 577 exclusion spheres mimicking the spatial constraints of the active site. Candidate compounds were retrieved if they mapped the three features with a Tversky_ref score above 0.6, leading to a final list of 2,519,562 candidate structures. (b) In PHARMER [50], the four-point pharmacophore models are characterized by their class, their position specified in Cartesian coordinates and a radius of 1 Å for the three hydrophobic/aromatic features and 3 Å for the exclusion sphere representing the tolerance spheres to search around this position.

PHARMER uses a root mean squared deviation (RMSD)-based method to rank the distance of the feature group of the screened molecule to the pharmacophore feature center. A set of 36,290 compound candidates was retrieved from the screening collections. (c) PepMMsMIMIC is a web server dedicated to peptidomimetic compound virtual screening based on a multi-conformers three-dimensional (3D)-similarity search strategy (<http://mms.dsfarm.unipd.it/pepMMsMIMIC>) [51]. The web service allows the screening of a library of 17 million conformers calculated from 3.9 million commercially available chemicals collected in the MMsINC[®] database. At our request, PepMMsMIMIC's authors also kindly expanded their database with the ChemBridge's EXPRESS-Pick collection. Starting from the crystal structure of PfAMA1–PfRON2sp1 complex (PDB code 3ZWZ) and the three-point pharmacophore model, commercial molecules were ranked using the combined shape (40 %) and pharmacophoric fingerprint similarity (60 %) score. As a result, we selected the best top 1000 peptidomimetic candidates from ChemBridge's EXPRESS-Pick collection and the best top 200 molecules from MMsINC[®] database.

Fig. 1 Graphical representation of the workflow of the ligand- and structure-based virtual screening



Docking as secondary filter

The *Pf*AMA1–*Pf*RON2sp1 co-structure (PDB code 3ZWZ) was used as the protein target structure in docking experiments with the PLANTS program [52]. All waters and ligand molecules were removed. Protons were assigned automatically at pH 7 by the program reduce (version 3.14) [53]. PLANTS is a semi-rigid docking program where the ligands are treated as flexible and the proteins as rigid. Multiple orientations of the ligand are sampled. Input structures and parameters files were generated by using LEA3D tools [54]. The binding site was a sphere of 12 Å centered on the oxygen atom of the side chain of Tyr-251. No water molecules were included in the binding site. PLANTS (version 1.1.) was used to generate ten poses with the ChemPLP score function. For the subsequent step, the best-scoring pose was selected.

Interaction checking and molecular visualization

The binding poses from PLANTS were analyzed through LIGPLOT [55] for their interaction with *Pf*AMA1 residues Tyr-234, Phe-183 and Val-169 which are in direct contact with the pharmacophore features. The PyMOL Molecular Graphic System, Version 1.5.0.4 Schrödinger, LLC was used for all molecular visualizations and image rendering.

PPI-HitProfiler

All selected compounds were profiled using the program PPI-HitProfiler to ensure that they were compliant with protein–protein interaction inhibitor's chemical space [56].

Peptides synthesis (Table 1)

The fluorescein-labeled peptide F**Pf*RON2sp1 was purchased from Kinexus (Vancouver, Canada). Unlabeled *Pf*RON2sp1, R1, fluorescein-labeled peptides F*R1, F*R1-13A1 and F**Pf*RON2sp3 were purchased from GeneCust Europe (Dudelange, Luxembourg) with a purity $\geq 95\%$.

Table 1 Peptides used in FA assay labeled with 5-carboxyfluorescein (5-FAM, F). For the shorter ligands, aminohexanoic acid (Ahx) was used as linker or spacer between the peptide and 5-FAM

Peptide	Sequence
Unlabeled <i>Pf</i> RON2sp1 (39 aa)	DITQAKDIGAGPVASCFTTRMSPPQIQCLNSVVNTALS
F* <i>Pf</i> RON2sp1 (39 aa)	5-FAM-DITQAKDIGAGPVASCFTTRMSPPQIQCLNSVVNTALS
F* <i>Pf</i> RON2sp3 (25 aa)	5-FAM-Ahx-KDIGAGPVASCFTTRMSPPQIQCLN
Unlabeled R1 (20 aa)	VFAEFLPLFSKFGSRMHILK
F*R1 (20 aa)	5-FAM-Ahx-VFAEFLPLFSKFGSRMHILK
F*R1-13A1 (13aa)	5-FAM-Ahx-ALPLFSKFGSRMH

Recombinant protein production *Pf*AMA1 (108–441)

A codon-optimized gene encoding DI and DII of *Pf*AMA1 3D7 [57] (residues 104–438; numbering based on the initiation methionine in the signal sequence, PF11_0344) was synthesized by GenScript and subcloned into a modified pAcGP67B vector (Pharming) for expression in insect cells using established protocols [17, 37]. *Pf*AMA1-His was purified by Ni-affinity chromatography, cleaved with thrombin to remove the hexa-histidine tag, further purified by size exclusion chromatography, and concentrated to 4.5 mg/mL for use in biophysical assays. Final yield of recombinant protein was approximately 3 mg/L of culture.

Fluorescence anisotropy

All measurements were carried out in PBS buffer at pH of 7.4; on 96-well, black, flat microplates, made of a non-binding surface (NBS) polystyrene nonionic hydrophilic surface (Cat No. 3993; Corning, Amsterdam, Netherlands). The temperature inside the wells was carefully measured with a thermocouple VWR traceable[®] (–200 to +1370 °C) with an error range of ± 0.1 °C. Data acquisition was carried out on a Wallac 2103 HTS Microplate EnVision Reader, PerkinElmer (Wallac Oy) operated by Wallac EnVision Manager 1.12. The anisotropy (r) and total fluorescence (F) values were measured and stored in spreadsheets. The instrument was equipped with an EnVision-2102 temperature control; Hamamatsu photomultiplier tube (R10130-10, serial No. AP7666); UV-Xenon fast tube lamp with spectral range 230–1100 nm; an optical module (481 FITC FP, D505fp/D535, diameter 150 mm), containing: 480 nm excitation filter (X480, band width 30 nm, 70 % T, diameter 150 mm), 535 nm S orientated emission filter (band with 40 nm, 80 % T, 150 mm), 535 nm P orientated emission filter (band with 40 nm, 80 % T, diameter 150 mm). Scans were carried out by row-bi-directional, ten flashes, 5–6 mm height, with a G factor of 1.04 and 750 PMT gain.

to prevent fluorescence quenching. *Pf*RON2sp1, F**Pf*RON2sp1 and F**Pf*RON2sp3 were disulfide cyclized

Titration experiments (Fig. S1a)

Titration experiments for K_D determination were carried out at 25 °C with a constant concentration of labeled probe (10 nM) titrated with increasing amounts of protein (0–10 μ M). Titration data was fitted by nonlinear regression model embedded in a simplex minimization routine solving the quadratic version of Eq. 1 where Y is the fraction saturation, X_T is total labeled peptide ($F^*PfRON2sp1$, $F^*PfRON2sp3$, F^*R1 or $F^*R1-13A1$), P and P_T are unbound and total protein ($PfAMA1$), respectively. Notice, that Eq. 1 is written in terms of increasing protein concentration, which titrates a constant amount of labeled ligand.

$$Y = \frac{[P]}{K_D + [P]} = \frac{[P_T] - [PX]}{K_D + ([P_T] - [PX])} \quad (1)$$

$$= \frac{(P_T - Y * X_T)}{K_D + (P_T - Y * X_T)}$$

Fluorescence anisotropy inhibition assay (Fig. 4)

Inhibition experiments were carried out with the peptide $F^*R1-13A1$. Preformed 150 μ L complex aliquots of 500 nM $PfAMA1$ and 10 nM $F^*R1-13A1$ were incubated for 20 min on the plate before adding the selected inhibitor candidates at concentrations of 20 μ M for a primary screening carried out in triplicate. A secondary screening was carried out to confirm hits at 20 and 40 μ M increasing the number of samples to 6 instead of 3 in the first screening. These two concentrations correspond to 0.25 and 0.50 % DMSO, respectively. To prevent systematic errors, samples were distributed in the 96-well plate according to a defined distribution pattern [58]. The data collection was carried out at incubation times of 1, 2, 3 h and overnight. The percentage of inhibition was calculated according to Eq. 2 [59]:

$$\%inhibition = 100 * \left(1 - \frac{r_{(complex+compound)} - r_{Free}}{r_{complex} - r_{Free}} \right) \quad (2)$$

where r_{free} , $r_{complex}$ and $r_{complex+compound}$ are the anisotropy signals of unbound labeled peptide, complex and complex-inhibitor mixture, respectively.

The concentration required for 50 % inhibition (IC_{50}) was investigated for peptide R1 and compound 3 and was determined from a sigmoid dose–response curve (Fig. S1b and Fig. 6) [60].

Surface plasmon resonance (Fig. 5)

SPR measurements were performed on a T200 apparatus (GE Healthcare). $PfAMA1$ proteins were covalently immobilized (17000 RU) on CM7 sensor chips (GE Healthcare) by an amine coupling procedure according to the

manufacturer's instructions. A reference flowcell was obtained with the same chemical treatment without $PfAMA1$. Binding assays of the different compounds were performed at 25 °C in HBS-EP + (GE Healthcare) containing 3 % DMSO. For ranking analysis each samples (0 and 50 μ M; Fig. 5a) were injected for 60 s followed by a 200 s dissociation phase at a flow rate of 30 μ L/min. $PfRON2sp1$ was injected as the positive ligand to check the response stability of the coated surface at the beginning and end of the experiment. Concentrations ranging from 25 to 200 μ M and 25 to 400 μ M for compound 3 and 8, respectively, were injected on immobilized $PfAMA1$ for dose–effect analysis (Fig. 5b). Each experimental series included blanks (running buffer) and solvent corrections. Results were analyzed by subtracting the signal of the reference flowcell from the signal of the $PfAMA1$ -bound flowcell using BiaEvaluation 4:1 software (GE Healthcare).

Results and discussion

Screening work-flow

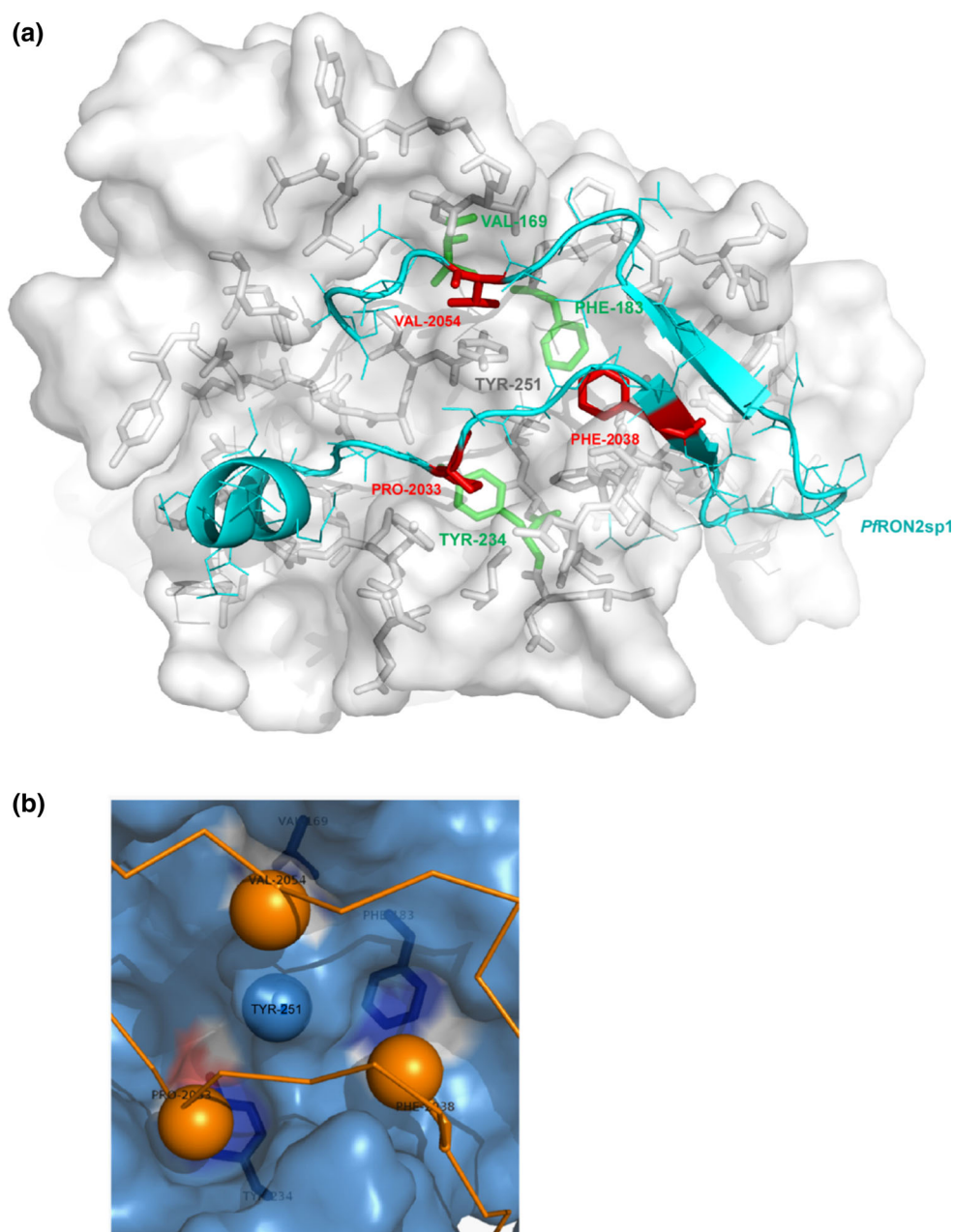
Here we report a $PfAMA1$ tailored workflow that involves two consecutive steps: ligand- and structure-based virtual screenings (Fig. 1). In both steps we used structural information for the $PfRON2sp$ and R1 peptides, conformation and interactions, derived from crystal structures (PDB code 3ZWZ and 3SRJ, respectively). Our pharmacophore models represent the spatial configuration of $PfAMA1$ – $PfRON2sp1/PfRON2sp2/R1$ protein–ligand interaction sites (also called features) in three-dimensional space. A minimum number of features have to be defined in order to efficiently represent a specific binding pattern and to successfully capture new active molecules. The ligand-based virtual screening was performed using three different in silico pharmacophore mapping programs: PHARMER [50], Align-it [49] and PepMMsMIMIC [51]. Pharmacophore search programs have been shown equally good in terms of percentage of enrichment of active compounds among first hits when challenged with benchmark compound set (actives + decoys) [61]. However, hits did not necessarily overlap because programs use different approaches with varying degrees of stringency. Therefore, increasing success may result from the combination of several programs. Vulliez-Le Normand et al. [62] showed by alanine scanning mutagenesis that mutations of Phe-183 and, to a lesser extent of Tyr-234, in $PfAMA1$ have an effect on binding. Similarly, mutagenesis highlighted four critical residues in $PfRON2$: Pro-2033, Phe-2038, Arg-2041 and Pro-2044. Of these, Pro-2033 and Phe-2038 are close to $PfAMA1$ key residues Tyr-234 and Phe-183, respectively (Fig. 2a). Additionally, Pro-2033 and Phe-2038

align structurally with Leu-6 and Phe-12 of peptide R1, respectively, highlighting the importance and the physicochemical nature of these anchoring residues (PDB 3SRJ). Therefore, in addition to Pro-2033 and Phe-2038 pharmacophore points, we selected a third hydrophobic feature that likely contributes to the binding between *Pf*AMA1 and *Pf*RON2. Indeed, Val-2054 of *Pf*RON2sp1 occupies a hydrophobic pocket at the opposite of the Pro-2033 pocket and is mimicked by Leu-8 in the R1 peptide. This constituted our three-point pharmacophore. Finally, an additional constraint was imposed in PHARMER by the way of an exclusion volume representing Tyr-251 that

protrudes from the surface of the *Pf*AMA1 binding groove in the middle of the three-point pharmacophore (Fig. 2b).

Our screening strategy used several collections that were expanded independently through generation of representative conformations, leading to a final sum of over 200,000,000 structures. The libraries overlap, at least in part [63, 64], but each collection has its own interest: diverse sets, proprietary compounds or focused libraries like the ChEMBL Malaria [65] and approved drugs (e-Drug3D) [46]. The ligand-based step filtered out 98.75 % of the input and retrieved over 2.5 million structures. The resulting list was further filtered by docking to the crystal

Fig. 2 Graphical representation of the four-point pharmacophore. **a** *Pf*AMA1 surface and pocket residues are colored in *white* and co-crystallized *Pf*RON2sp1 backbone is colored in *cyan*. *Pf*AMA1 hotspots are colored in *green* and *Pf*RON2sp1 interacting residues are colored in *red*. **b** Pharmacophore model inside the binding pocket (*orange*: matching features, *blue*: exclusion sphere)



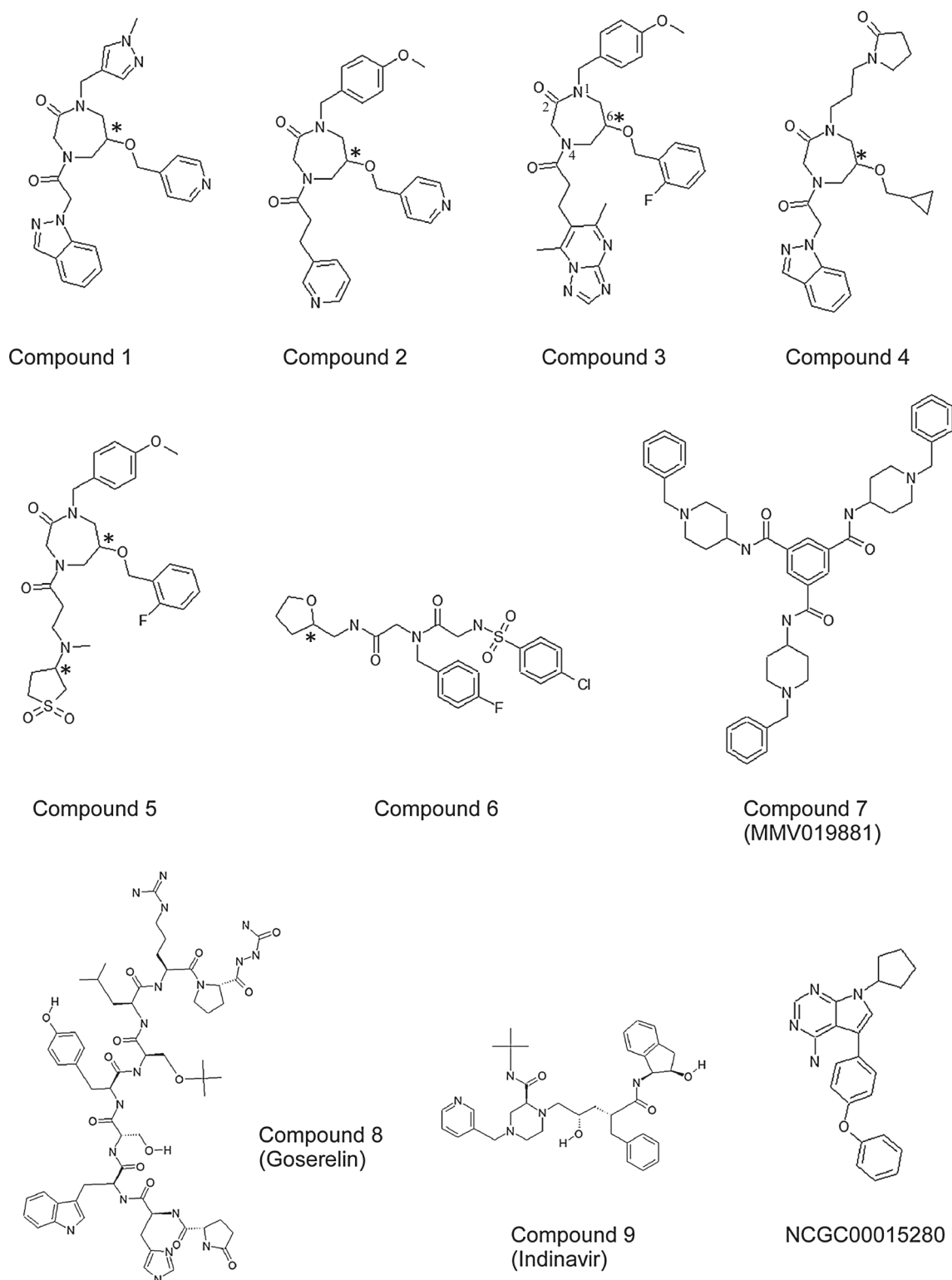


Fig. 3 Structures of 10 experimentally tested hits. Compounds 1–6 and compounds 8 and 9 result from the application of the screening workflow. Compound 7 comes from the docking of the Malaria Box against the experimental structure of *Pf*AMA1. NCGC00015280 is a

published inhibitor of *Pf*AMA1–*Pf*RON2 interaction [22]. Carbon stereocenters are indicated by a *star*. Atom numbering of the 1,4-diazepin-2-one scaffold is indicated for compound 3

structure of *Pf*AMA1 (PDB code 3ZWZ) by using PLANTS [52]. We then used LIGPLOT to select those that dock into the groove while interacting with the three key residues Tyr-234, Phe-183 and Val-169. This second step filtered out 99.72 % of docked compounds leading to 7161 structures. However, due to low throughput assays at that time, we had to stringently inspect and prioritize remaining candidates. We visually checked the superimposition of the molecular envelope of candidate inhibitors with the 3D shape of *Pf*RON2sp1 and favored molecules possessing an aromatic ring mimicking *Pf*RON2sp1 Phe-2038. As we proceeded, we realized that few structural families possess these characteristics. Finally, we selected and purchased 8 potential inhibitors representing approximately one-in-a-million of the screened collections (compound 1–6 and compounds 8 and 9 in Fig. 3). In addition, given the size of the Malaria Box (400 compounds), we directly carried out the docking of this library against *Pf*AMA1 leading to the selection of one commercially available candidate (compound 7, MMV019881). Finally, we investigated the compliance of our compound selection with some physicochemical parameters related to known inhibitors of protein–protein interactions by using the program PPI-HitProfiler [56]. As a result, all compounds positively featured characteristics of known PPI inhibitors such as high number of aromatic rings, high number of multiple bonds and spatial distribution around a central scaffold [66].

On closer inspection of these nine selected molecules, compounds 1–5 belong to the same structural class of 1,4-diazepin-2-one which possess three substituents at position 1, 4 and 6 (Fig. 3, compound 3). With the exception of compound 2, both PHARMER and Align-it tools selected the same structural class but not the same structures (Table 2). Compound 8 (Goserelin) is a FDA approved gonadotropin releasing hormone (GnRH) agonist whereas compound 9 (Indinavir) is a HIV protease inhibitor. Interestingly, studies on the antimalarial activity of Indinavir suggested the existence of *Plasmodium falciparum* targets but did not identify them [67]. An a posteriori analysis of the different chemotypes present among the structure-based hits showed that four selected compounds (compounds 2, 3, 5 and 8) fell into three clusters among the 20 most populated ones (Fig. S5). Comparing ligand-based methods, this analysis also showed that 7 out of 9 selected compounds represent chemotypes that have been selected both by PHARMER and Align-it methods.

Development of a fluorescence anisotropy binding assay for *Pf*AMA1

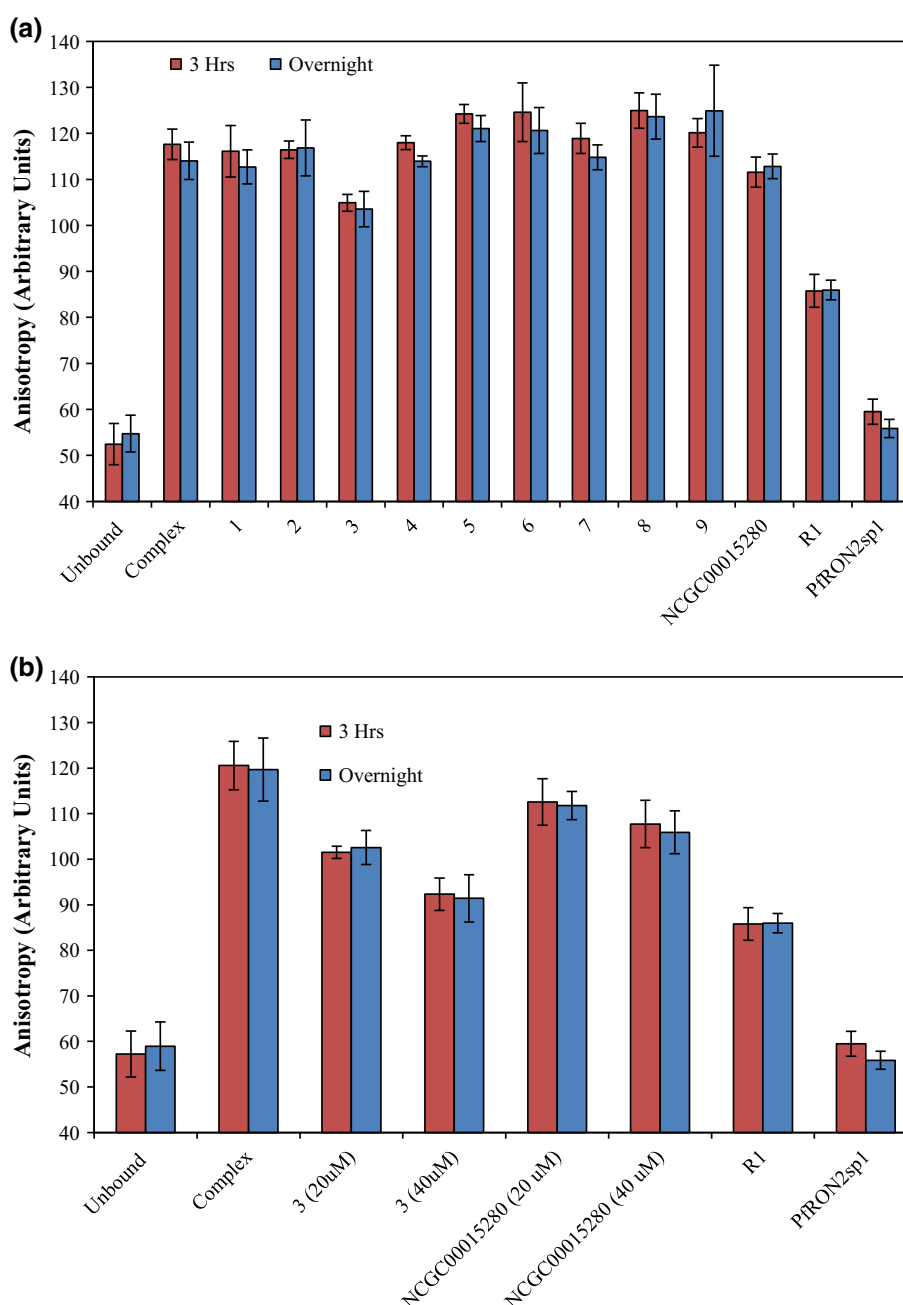
In order to test candidate inhibitors, we developed a sensitive competition assay based on fluorescence anisotropy signal

Table 2 In silico and experimental validation of the 11 tested molecules by FA-based assay (at concentration of 20 μ M), SPR and IC₅₀ (neg.: negative; n.d.: not determined)

Compound	Ligand-based method	Chemical collection	Plants score value	Pharmacophore match	First screening FA assay (% of complex inhibition)	SPR	IC ₅₀ (μ M)
Reference		R1	n.d.	x	83 at 100 nM	[80–177] nM [15]	0.164
1	PHARMER	CombiLib	–101.03	x	Neg.	Neg.	n.d.
2	Align-it ZINCPHARMER	ZINC	–95.3	x	Neg.	Neg.	n.d.
3	PHARMER	CombiLib	–94.46	x	28.2	Positive (moderate solubility)	24
4	Align-it	CombiLib	–90.26	x	Neg.	Neg.	n.d.
5	Align-it	CombiLib	–98.75	x	Neg.	Neg.	n.d.
6	ZINCPHARMER	ZINC	–109.27	x	Neg.	Neg.	n.d.
7	Docking	MalariaBox MMV019881	–91	x	Neg.	Neg.	n.d.
8	PHARMER	e-Drug3D Goserelin	–140.46	x	Neg.	Positive (moderate solubility)	n.d. (moderate solubility)
9	Align-it	e-Drug3D Indinavir	–101.06	x	Neg.	Inconclusive	n.d. (moderate solubility)
	Literature [14]	NCGC00015280	–79.47	No	13	Positive (low solubility)	n.d. (aggregation)

^a Contacting the pharmacophore features Tyr-234, Phe-183 and Val-169

Fig. 4 a Inhibition competition primary screening of inhibitor candidates by fluorescence anisotropy at 22 °C after 3 h and overnight incubation. Complex was incubated for 20 min following the addition of inhibitor candidates (20 μ M). Medium and strong positive controls were prepared adding to the complex unlabeled R1 (100 nM) and *Pf*RON2sp1 (1 μ M), respectively. Complex in 0.25 % DMSO was used as the negative control. Assay was performed in triplicate with the error bars corresponding to 1 standard deviation. Compound 3 and NCGC00015280 were possible hits and were further tested. **b** Inhibition competition secondary screening at 20 and 40 μ M at 22 °C with six samples per concentration. Error bars correspond to 1 standard deviation



changes (FA) that follows a binding event between *Pf*AMA1 and a ligand. This assay requires a labeled probe with a relative weak K_D to facilitate its displacement by a non-optimized small size candidate inhibitor. Indeed, the affinity of known peptide inhibitor F**Pf*RON2sp1 for *Pf*AMA1 is in the nanomolar range [17] and is too high to observe displacement with our candidate inhibitors. Therefore, we first designed and tested a truncated and modified version of F**Pf*RON2sp1, called F**Pf*RON2sp3, which resulted in a peptide with 5.4-fold weaker K_D of 92.2 nM at 25 °C (Table 1 and Fig. S1a). As the affinity of F**Pf*RON2sp3 was

still too high, we then tested a shortened 13 amino acid analog of the R1 peptide { $K_D = (80–177)$ nM [15, 17, 40, 41]} that was generated based on the analysis of the three-dimensional crystal structure (PDB code 3SRJ) [17]. This peptide, called F*R1-13A1, was obtained by removing N-terminal and C-terminal amino acids of R1 and by mutating Phe-5 into alanine (Table 1). Our objective was to affect the affinity without compromising the overall binding paradigm. Indeed, Phe-5 is an anchor point of R1 occupying a hydrophobic pocket [17, 41] that is otherwise filled by Phe-367 of the DII loop in the apo form of *Pf*AMA1 (PDB code 1Z40)

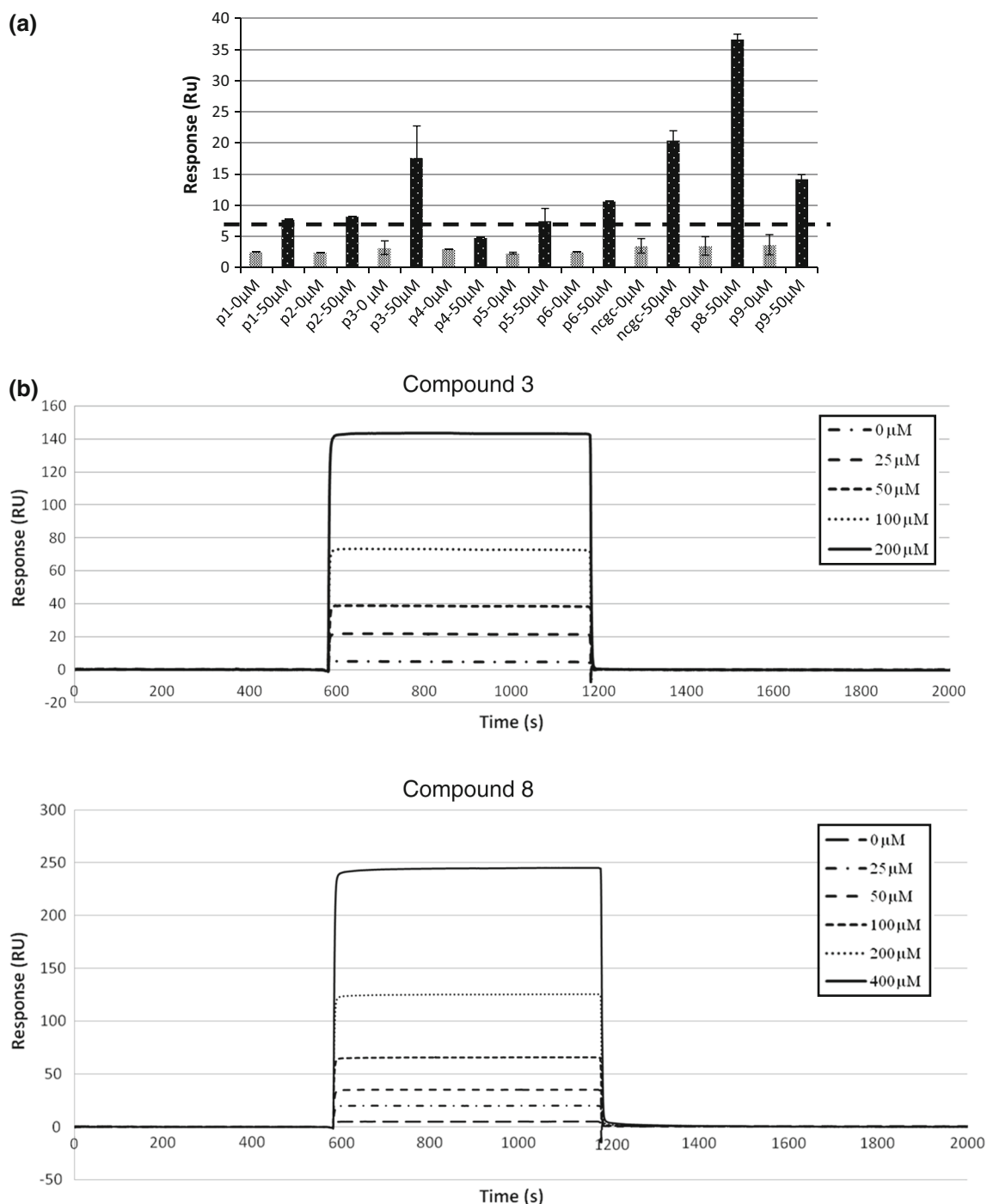


Fig. 5 Surface plasmon resonance studies of candidate inhibitors. **a** The binding responses obtained by the injection of the different molecules on immobilized *Pf*AMA1 are plotted as bars along the x axis. Grey and black bars represented 0 and 50 μM responses, respectively. The dashed line is the threshold value corresponding to three times the

average of buffer responses (8.8 RU). Compounds 3 and 8 were positive hits whereas sensorgrams revealed the limit solubility of compound 9 and NCGC00015280 (ncgc). **b** Sensorgrams of compounds 3 and 8 indicated a binding event with *Pf*AMA1 but saturation is not obtained likely due to an aggregation at high concentration

and left vacant when the DII loop is displaced. The K_D of F*R1-13A1 peptide was measured to be 422.3 nM at 25 °C which is 26-fold weaker than F**Pf*RON2sp1 and 2.9-fold weaker than F*R1 while binding the same pocket as R1 and

*Pf*RON2sp1 as shown in competitive binding experiments (Figs. S1a, b). This value is in agreement with the binding affinity of 990 nM that has been recently obtained by SPR for the closest published truncated peptide R1_{5–16} [40].

Biochemical evaluation of inhibitor candidates

The nine selected compounds were then validated experimentally using the FA-based inhibition assay to determine their ability to disrupt the *Pf*AMA1–F*R1-13A1 complex. The recently published *Pf*AMA1–*Pf*RON2 inhibitory molecule NCGC00015280 (Fig. 3) was also investigated [22] although in our model the docked pose for this compound did not overlap the three-point pharmacophore. We checked DMSO effect (up to 1 %) as well as complex stability in overnight incubation (Fig. S2) because of the slow complex dissociation process observed for the native complex *Pf*AMA1–*Pf*RON2sp1 (Fig. S3). The assay showed a very good Z' -value from 0.60 up to 0.77. A Z' -value of 0.5 is acceptable and used to determinate the optimal signal window and assay discrimination capabilities [68]. Compounds 3 and NCGC00015280 showed moderate complex disruption (Fig. 4a) in the first screening with triplicate samples at 20 μ M. Therefore, a secondary screening was carried out with six samples at 20 and 40 μ M (Fig. 4b) confirming the inhibition potency of compound 3 and NCGC00015280.

Since each biophysical technique has limitations, binding affinities were also measured by SPR. The binding of compound 3 and NCGC00015280 to *Pf*AMA1 were confirmed (Fig. 5), but as compound 3 failed to saturate (Fig. 5b) and the sensorgram for NCGC00015280 showed a low solubility profile type (data not shown), the estimation of the apparent equilibrium dissociation constants K_D was precluded. SPR analysis also showed binding with candidates 8 and 9 (Fig. 5a, b) though the binding with candidate 9 at 50 μ M was inconclusive (Fig. 5a). However, since these two compounds were not positive hits in FA-based assay, we did not characterize them further.

Dose–response experiments were then investigated using the fluorescence anisotropy change and IC_{50} values was measured to be of 24 μ M ($\pm 2 \mu$ M) for compound 3 (Fig. 6). On the contrary, IC_{50} for NCGC00015280 was not measurable due to the scattering of light when concentration exceeded 50 μ M (data not shown). This aggregation phenomenon was also reported by Devine et al. [23]. Compound 3 showed a moderate affinity but it had been tested as a racemic mixture whereas the R enantiomer only had been selected by virtual screening. The carbon stereocenter at position 6 of the 1,4-diazepin-2-one ring is indicated by a star in Fig. 3. We would expect a better IC_{50} for this enantiomer if tested separately.

The predicted docked pose of compound 3 is shown in Fig. 7a, b. Aromatic ring groups (green sticks) are overlapping key interacting residues of *Pf*RON2sp1 (red sticks) directly in contact with hotspots (white sticks) of *Pf*AMA1 (white surface). Its interactions with *Pf*AMA1 involves: (1) A π -stacking between the [1, 2, 4] triazolo[1,5-

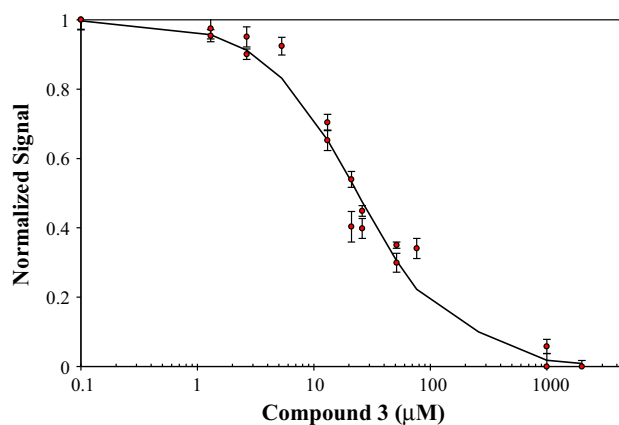


Fig. 6 Competition binding experiment between F*R1-13A1 and compound 3 using 600 nM of *Pf*AMA1, 10 nM of F*R1-13A1 and an increasing concentration of candidate compound. The mixture was incubated for 3 h at 20 °C. The corresponding IC_{50} for compound 3 was measured to be 24 μ M ($\pm 2 \mu$ M)

a]pyrimidin-6-yl group with Tyr-142, Tyr-234 and Tyr-251; this group is predicted to mimic Pro-2033 of *Pf*RON2sp1 and superimposes well with Lys-368 of the DII loop when it packs against the groove (PDB 1Z40); (2) A hydrogen bond between the carbonyl of the oxopropyl with the hydroxyl of Tyr-236; (3) A π -stacking between the fluorophenyl ring with key residue Phe-183; this ring is predicted to mimic Phe-2038 of *Pf*RON2sp1 and superimposes with Phe-12 of R1 (PDB 3SRJ); (4) A π -stacking between the methoxyphenyl ring with Tyr-251; This substituent is predicted to mimic Val-2054 of *Pf*RON2sp1 (or Leu-8 of R1 (PDB 3SRJ)).

Compounds 1–5 overlap well with the three-point pharmacophore due to their star-shaped structure (Fig. S4). Only one enantiomer of each compound was present in our results whereas commercial products are racemic mixtures. This family of structures has been designed and synthesized by Chembrige Corporation but has not yet been associated with any biological activity. Comparing docking poses of these five candidates revealed that compound 3 overlaid the best with *Pf*RON2sp1. It is noteworthy that compound 3 mimics Pro-2033 and was the only selected compound able to form a parallel π -stacking arrangement with Tyr-142 and Tyr-251. Compound 1, 2 and 3 possess three aromatic substituents whereas compounds 4 and 5 have two or one non aromatic substituents, respectively. Compound 1 superimposes well with compound 3 but the substituent at position 4 has a linker with one carbon shorter and the connected ring plane is perpendicular to Tyr-142 and Tyr-251. Compound 2 is the compound that overlaid the worst with compound 3 because of a flip that superimposes the substituent at position 1 with substituent at position 6, respectively. The relative enantiomer at position 6 is

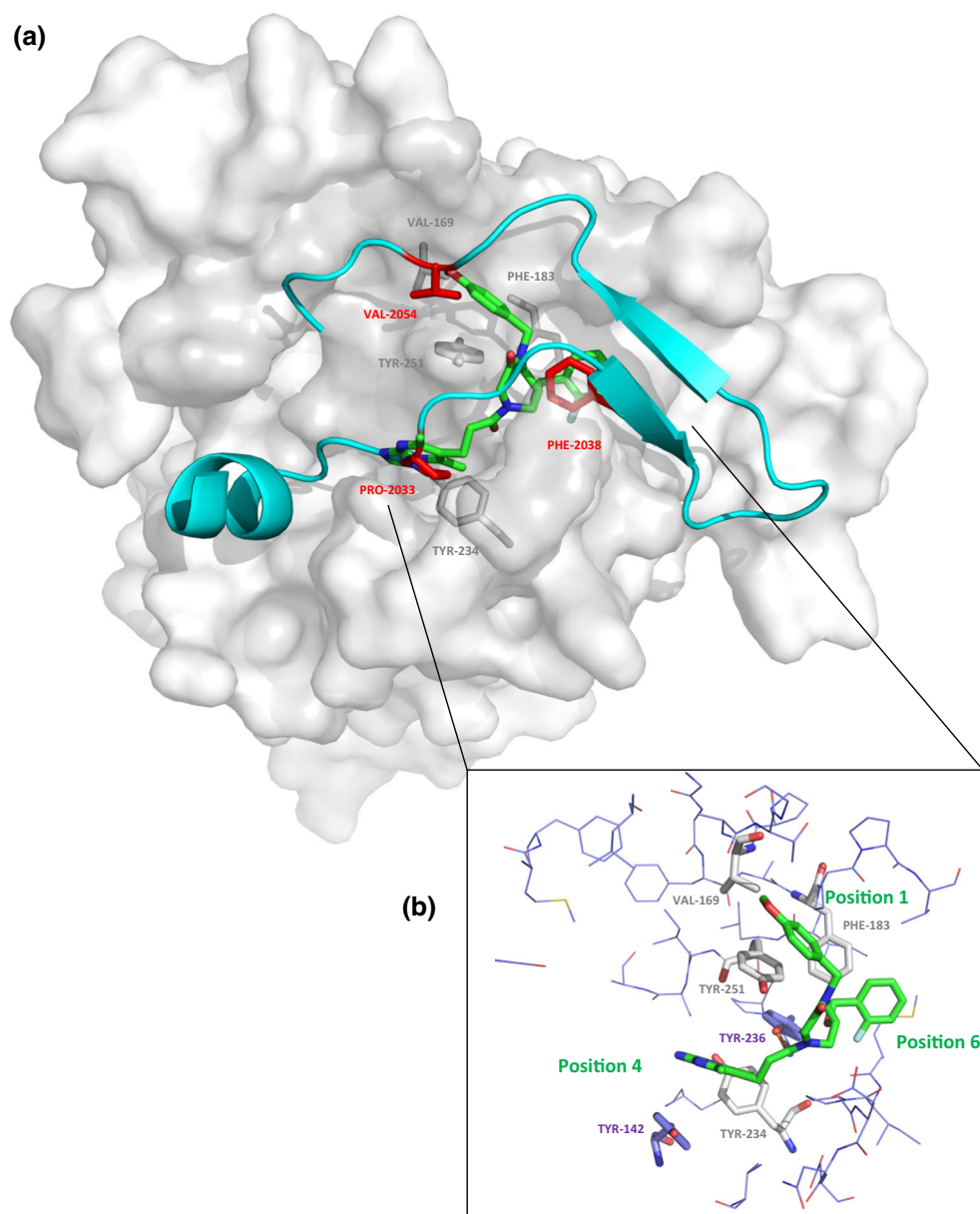


Fig. 7 **a** Predicted binding mode of compound 3 (carbon atoms in green) in the groove of *PfAMA1* (white surface and side-chains of hotspots in sticks). Co-crystallized *PfRON2sp1* backbone is colored in cyan and the three-point pharmacophore side chains are in red. Labels of key residues are indicated in red and grey for *PfRON2sp1* and *PfAMA1*, respectively. **b** A close view of the interactions

between *PfAMA1* and compound 3. A hydrogen bond is depicted in orange between the hydroxyl of Tyr-236 and carbonyl of the oxopropyl of compound 3. *PfAMA1* residues in white (hotspots) and blue are predicted to interact with compound 3. Position number of substituents on the 1,4-diazepin-2-one scaffold are indicated in green

inverted when compared with compound 3. Compound 4 possesses a linker with one carbon shorter at position 4 and the ring at position 6 is not aromatic. Finally, compound 5 is different from compound 3 by its substituent at position 4 that led us to suggest that an aromatic or cationic group at this sub-site lined by aromatics (Tyr-142, Tyr-234, Tyr-236 and Tyr-251) is required for binding of a non-peptide inhibitor. This feature may be as important as the presence of a π -stacking with Phe-183.

The nature of the *PfAMA1*–*PfRON2* interface with its extensive, but relatively deep, solvent accessible groove and the presence of *PfAMA1* DII loop make it a challenging target for traditional drug discovery. The structural family of 1,4-diazepin-2-one provides multiple and widely spaced hydrophobic groups predicted to interact with the *PfAMA1*–*PfRON2* hotspots. However, based on our results, it is clear that the R enantiomer of compound 3 must be tested separately and, if conclusive, be modified to make

additional polar interactions with other *Pf*AMA1 sub-sites as well as with the surrounding water molecules. These candidates are rather large but it will not necessarily hinder their optimization since reported PPI inhibitors tend to be larger in molecular weight than drug-like molecules [66, 69] and often violate Lipinski's 'rule of five' [29, 70]. As an extreme example, the phase II candidate Navitoclax is orally bioavailable despite its molecular weight of 974 [71]. When working with PPI inhibitors, the traditional drug-like chemical space must be expanded to borderline molecules and it is now accepted that existing compound libraries are not yet sufficiently populated with complicated (larger and more three-dimensional) molecules [26].

Conclusions

In the present work, we aimed at exploiting both mutagenesis and structural data of the target protein *Pf*AMA1 to explore a large set of molecules for *Pf*AMA1–*Pf*RON2 complex inhibition by an integrated computational and biophysical approach. Nine small molecules were selected with respect to their predicted interactions with key residues Val169, Phe183 and Tyr234 and their commercial availability for biological evaluation. We showed that FA and SPR assays were able to corroborate the moderate binding of published NCGC00015280 and to establish an IC_{50} of 24 μ M for compound 3 to *Pf*AMA1. These experimental data must be now validated by a co-crystallization study with *Pf*AMA1 protein to obtain structural information about the binding mode that can be used to logically direct the design of more potent inhibitors. Such results would support the validity of our virtual screening protocol and allow us to screen and select other families of compounds for a second experimental screen. We also anticipate that more positive hits may be found if a specific chemical library dedicated to inhibit PPI was screened.

Acknowledgments This work was supported by the Centre National de la Recherche Scientifique (CNRS), the Agence Nationale de la Recherche (ANR-12-BSV3-0012-03) and l'Institut National de la Santé et de la Recherche Médicale (INSERM) to DD and by the Canadian Institutes of Health Research (CIHR) Grant MOP82915 to MJB. We thank CONACYT postdoctoral fellowships (130994, 162809) and Veracruz scholarship for RFD. We thank Damien Barbier and Corinne Henriquet for technical supports.

References

- Organization WH (2013) World malaria report 2012
- Bright AT, Winzeler EA (2013) Epidemiology: resistance mapping in malaria. *Nature* 498(7455):446–447. doi:10.1038/498446b
- Aikawa M, Miller LH, Johnson J, Rabbege J (1978) Erythrocyte entry by malarial parasites. A moving junction between erythrocyte and parasite. *J Cell Biol* 77(1):72–82
- Besteiro S, Dubremetz JF, Lebrun M (2011) The moving junction of apicomplexan parasites: a key structure for invasion. *Cell Microbiol* 13(6):797–805. doi:10.1111/j.1462-5822.2011.01597.x
- Riglar DT, Richard D, Wilson DW, Boyle MJ, Dekiwadia C, Turnbull L, Angrisano F, Marapana DS, Rogers KL, Whitchurch CB, Beeson JG, Cowman AF, Ralph SA, Baum J (2011) Super-resolution dissection of coordinated events during malaria parasite invasion of the human erythrocyte. *Cell Host Microbe* 9(1):9–20. doi:10.1016/j.chom.2010.12.003
- Cao J, Kaneko O, Thongkukiattkul A, Tachibana M, Otsuki H, Gao Q, Tsuboi T, Torii M (2009) Rhoptry neck protein RON2 forms a complex with microneme protein AMA1 in *Plasmodium falciparum* merozoites. *Parasitol Int* 58(1):29–35. doi:10.1016/j.parint.2008.09.005
- Besteiro S, Michelin A, Poncet J, Dubremetz JF, Lebrun M (2009) Export of a *Toxoplasma gondii* rhoptry neck protein complex at the host cell membrane to form the moving junction during invasion. *PLoS Pathog* 5(2):e1000309. doi:10.1371/journal.ppat.1000309
- Lamarque M, Besteiro S, Papoin J, Roques M, Vulliez-Le Normand B, Morlon-Guyot J, Dubremetz JF, Fauquenoy S, Tomavo S, Faber BW, Kocken CH, Thomas AW, Boulanger MJ, Bentley GA, Lebrun M (2011) The RON2-AMA1 interaction is a critical step in moving junction-dependent invasion by apicomplexan parasites. *PLoS Pathog* 7(2):e1001276. doi:10.1371/journal.ppat.1001276
- Tyler JS, Boothroyd JC (2011) The C-terminus of *Toxoplasma* RON2 provides the crucial link between AMA1 and the host-associated invasion complex. *PLoS Pathog* 7(2):e1001282. doi:10.1371/journal.ppat.1001282
- Srinivasan P, Beatty WL, Diouf A, Herrera R, Ambroggio X, Moch JK, Tyler JS, Narum DL, Pierce SK, Boothroyd JC, Haynes JD, Miller LH (2011) Binding of *Plasmodium* merozoite proteins RON2 and AMA1 triggers commitment to invasion. *Proc Natl Acad Sci USA* 108(32):13275–13280. doi:10.1073/pnas.1110303108
- Lamarque MH, Roques M, Kong-Hap M, Tonkin ML, Rugarabamu G, Marq JB, Penarete-Vargas DM, Boulanger MJ, Soldati-Favre D, Lebrun M (2014) Plasticity and redundancy among AMA-RON pairs ensure host cell entry of *Toxoplasma* parasites. *Nat Commun* 5:4098. doi:10.1038/ncomms5098
- Yap A, Azevedo MF, Gilson PR, Weiss GE, O'Neill MT, Wilson DW, Crabb BS, Cowman AF (2014) Conditional expression of apical membrane antigen 1 in *Plasmodium falciparum* shows it is required for erythrocyte invasion by merozoites. *Cell Microbiol* 16(5):642–656. doi:10.1111/cmi.12287
- Harris KS, Casey JL, Coley AM, Masciantonio R, Sabo JK, Keizer DW, Lee EF, McMahon A, Norton RS, Anders RF, Foley M (2005) Binding hot spot for invasion inhibitory molecules on *Plasmodium falciparum* apical membrane antigen 1. *Infect Immun* 73(10):6981–6989. doi:10.1128/IAI.73.10.6981-6989.2005
- Richard D, MacRaid CA, Riglar DT, Chan JA, Foley M, Baum J, Ralph SA, Norton RS, Cowman AF (2010) Interaction between *Plasmodium falciparum* apical membrane antigen 1 and the rhoptry neck protein complex defines a key step in the erythrocyte invasion process of malaria parasites. *J Biol Chem* 285(19):14815–14822. doi:10.1074/jbc.M109.080770
- Harris KS, Casey JL, Coley AM, Karas JA, Sabo JK, Tan YY, Dolezal O, Norton RS, Hughes AB, Scanlon D, Foley M (2009) Rapid optimization of a peptide inhibitor of malaria parasite invasion by comprehensive N-methyl scanning. *J Biol Chem* 284(14):9361–9371. doi:10.1074/jbc.M808762200
- Tonkin ML, Roques M, Lamarque MH, Pugnieri M, Douguet D, Crawford J, Lebrun M, Boulanger MJ (2011) Host cell invasion by apicomplexan parasites: insights from the co-structure of AMA1 with a RON2 peptide. *Science* 333(6041):463–467. doi:10.1126/science.1204988

17. Vulliez-Le Normand B, Tonkin ML, Lamarque MH, Langer S, Hoos S, Roques M, Saul FA, Faber BW, Bentley GA, Boulanger MJ, Lebrun M (2012) Structural and functional insights into the malaria parasite moving junction complex. *PLoS Pathog* 8(6):e1002755. doi:10.1371/journal.ppat.1002755
18. Santos G, Torres NV (2013) New targets for drug discovery against malaria. *PLoS One* 8(3):e59968. doi:10.1371/journal.pone.0059968
19. Macrauld CA, Anders RF, Foley M, Norton RS (2011) Apical membrane antigen 1 as an anti-malarial drug target. *Curr Top Med Chem* 11(16):2039–2047
20. Remarque EJ, Faber BW, Kocken CH, Thomas AW (2008) Apical membrane antigen 1: a malaria vaccine candidate in review. *Trends Parasitol* 24(2):74–84. doi:10.1016/j.pt.2007.12.002
21. Srinivasan P, Ekanem E, Diouf A, Tonkin ML, Miura K, Boulanger MJ, Long CA, Narum DL, Miller LH (2014) Immunization with a functional protein complex required for erythrocyte invasion protects against lethal malaria. *Proc Natl Acad Sci USA* 111(28):10311–10316. doi:10.1073/pnas.1409928111
22. Srinivasan P, Yasgar A, Luci DK, Beatty WL, Hu X, Andersen J, Narum DL, Moch JK, Sun H, Haynes JD, Maloney DJ, Jadhav A, Simeonov A, Miller LH (2013) Disrupting malaria parasite AMA1–RON2 interaction with a small molecule prevents erythrocyte invasion. *Nat Commun* 4:2261. doi:10.1038/ncomms3261
23. Devine SM, Lim SS, Chandrashekar IR, MacRauid CA, Drew DR, Debono CO, Lam R, Anders RF, Beeson JG, Scanlon MJ, Scammells PJ, Norton RS (2014) A critical evaluation of pyrrolo[2,3-d]pyrimidine-4-amines as *Plasmodium falciparum* apical membrane antigen 1 (AMA1) inhibitors. *Med Chem Commun* 5(10):1500–1506
24. Ge X, MacRauid CA, Devine SM, Debono CO, Wang G, Scammells PJ, Scanlon MJ, Anders RF, Foley M, Norton RS (2014) Ligand-induced conformational change of *Plasmodium falciparum* AMA1 detected using 19F NMR. *J Med Chem* 57(15):6419–6427. doi:10.1021/jm500390g
25. Alam A (2014) Bioinformatic identification of peptidomimetic-based inhibitors against *Plasmodium falciparum* antigen AMA1. *Malar Res Treat* 2014:642391. doi:10.1155/2014/642391
26. Mullard A (2012) Protein-protein interaction inhibitors get into the groove. *Nat Rev Drug Discov* 11(3):173–175. doi:10.1038/nrd3680
27. Wendt MD (2008) Discovery of ABT-263, a Bcl-family protein inhibitor: observations on targeting a large protein–protein interaction. *Expert Opin Drug Discov* 3(9):1123–1143. doi:10.1517/17460441.3.9.1123
28. Wilson AJ (2009) Inhibition of protein–protein interactions using designed molecules. *Chem Soc Rev* 38(12):3289–3300. doi:10.1039/b807197g
29. Labbe CM, Laconde G, Kuenemann MA, Villoutreix BO, Sperandio O (2013) iPPI-DB: a manually curated and interactive database of small non-peptide inhibitors of protein–protein interactions. *Drug Discov Today* 18(19–20):958–968. doi:10.1016/j.drudis.2013.05.003
30. Ono K, Takeuchi K, Ueda H, Morita Y, Tanimura R, Shimada I, Takahashi H (2014) Structure-based approach to improve a small-molecule inhibitor by the use of a competitive peptide ligand. *Angew Chem Int Ed Engl* 53(10):2597–2601. doi:10.1002/anie.201310749
31. Anderson AC (2012) Winning the arms race by improving drug discovery against mutating targets. *ACS Chem Biol* 7(2):278–288. doi:10.1021/cb200394t
32. Bourgeas R, Basse MJ, Morelli X, Roche P (2010) Atomic analysis of protein-protein interfaces with known inhibitors: the 2P2I database. *PLoS One* 5(3):e9598. doi:10.1371/journal.pone.0009598
33. Pizarro JC, Vulliez-Le Normand B, Chesne-Seck ML, Collins CR, Withers-Martinez C, Hackett F, Blackman MJ, Faber BW, Remarque EJ, Kocken CH, Thomas AW, Bentley GA (2005) Crystal structure of the malaria vaccine candidate apical membrane antigen 1. *Science* 308(5720):408–411. doi:10.1126/science.1107449
34. Bai T, Becker M, Gupta A, Strike P, Murphy VJ, Anders RF, Batchelor AH (2005) Structure of AMA1 from *Plasmodium falciparum* reveals a clustering of polymorphisms that surround a conserved hydrophobic pocket. *Proc Natl Acad Sci USA* 102(36):12736–12741. doi:10.1073/pnas.0501808102
35. Coley AM, Gupta A, Murphy VJ, Bai T, Kim H, Foley M, Anders RF, Batchelor AH (2007) Structure of the malaria antigen AMA1 in complex with a growth-inhibitory antibody. *PLoS Pathog* 3(9):1308–1319. doi:10.1371/journal.ppat.0030138
36. Henderson KA, Streltsov VA, Coley AM, Dolezal O, Hudson PJ, Batchelor AH, Gupta A, Bai T, Murphy VJ, Anders RF, Foley M, Nuttall SD (2007) Structure of an IgNAR-AMA1 complex: targeting a conserved hydrophobic cleft broadens malarial strain recognition. *Structure* 15(11):1452–1466. doi:10.1016/j.str.2007.09.011
37. Crawford J, Tonkin ML, Grujic O, Boulanger MJ (2010) Structural characterization of apical membrane antigen 1 (AMA1) from *Toxoplasma gondii*. *J Biol Chem* 285(20):15644–15652. doi:10.1074/jbc.M109.092619
38. Tonkin ML, Crawford J, Lebrun ML, Boulanger MJ (2013) *Babesia divergens* and *Neospora caninum* apical membrane antigen 1 structures reveal selectivity and plasticity in apicomplexan parasite host cell invasion. *Protein Sci* 22(1):114–127. doi:10.1002/pro.2193
39. Lim SS, Yang W, Krishnarajuna B, Kannan Sivaraman K, Chandrashekar IR, Kass I, MacRauid CA, Devine SM, Debono CO, Anders RF, Scanlon MJ, Scammells PJ, Norton RS, McGowan S (2014) Structure and dynamics of apical membrane antigen 1 from *Plasmodium falciparum* FVO. *Biochemistry* 53(46):7310–7320. doi:10.1021/bi5012089
40. Wang G, MacRauid CA, Mohanty B, Mobli M, Cowieson NP, Anders RF, Simpson JS, McGowan S, Norton RS, Scanlon MJ (2014) Molecular insights into the interaction between *Plasmodium falciparum* apical membrane antigen 1 and an invasion-inhibitory peptide. *PLoS One* 9(10):e109674. doi:10.1371/journal.pone.0109674
41. Lee EF, Yao S, Sabo JK, Fairlie WD, Stevenson RA, Harris KS, Anders RF, Foley M, Norton RS (2011) Peptide inhibitors of the malaria surface protein, apical membrane antigen 1: identification of key binding residues. *Biopolymers* 95(5):354–364. doi:10.1002/bip.21582
42. Jubb H, Higuero AP, Winter A, Blundell TL (2012) Structural biology and drug discovery for protein–protein interactions. *Trends Pharmacol Sci* 33(5):241–248. doi:10.1016/j.tips.2012.03.006
43. Azzarito V, Long K, Murphy NS, Wilson AJ (2013) Inhibition of alpha-helix-mediated protein-protein interactions using designed molecules. *Nat Chem* 5(3):161–173. doi:10.1038/nchem.1568
44. Owicki JC (2000) Fluorescence polarization and anisotropy in high throughput screening: perspectives and primer. *J Biomol Screen* 5(5):297–306
45. Chuprina A, Lukin O, Demoiseaux R, Buzko A, Shivanyuk A (2010) Drug- and lead-likeness, target class, and molecular diversity analysis of 7.9 million commercially available organic compounds provided by 29 suppliers. *J Chem Inform Model* 50(4):470–479. doi:10.1021/ci900464s
46. Pihan E, Colliandre L, Guichou JF, Douguet D (2012) e-Drug 3D: 3D structure collections dedicated to drug repurposing and fragment-based drug design. *Bioinformatics* 28(11):1540–1541. doi:10.1093/bioinformatics/bts186
47. Hawkins PC, Skillman AG, Warren GL, Ellingson BA, Stahl MT (2010) Conformer generation with OMEGA: algorithm and

- validation using high quality structures from the Protein Data Bank and Cambridge Structural Database. *J Chem Inform Model* 50(4):572–584. doi:[10.1021/ci100031x](https://doi.org/10.1021/ci100031x)
48. Gasteiger J, Rudolph C, Sadowski J (1990) Automatic generation of 3D-atomic coordinates for organic molecules. *Tetrahedron Comput Method* 3:537–547
49. Taminau J, Thijs G, De Winter H (2008) Pharao: pharmacophore alignment and optimization. *J Mol Graph Model* 27(2):161–169. doi:[10.1016/j.jmgm.2008.04.003](https://doi.org/10.1016/j.jmgm.2008.04.003)
50. Koes DR, Camacho CJ (2011) Pharmer: efficient and exact pharmacophore search. *J Chem Inform Model* 51(6):1307–1314. doi:[10.1021/ci200097m](https://doi.org/10.1021/ci200097m)
51. Floris M, Masciocchi J, Fanton M, Moro S (2011) Swimming into peptidomimetic chemical space using pepMMsMIMIC. *Nucleic Acids Res* 39:W261–269. doi:[10.1093/nar/gkr287](https://doi.org/10.1093/nar/gkr287) (Web Server issue)
52. Korb O, Stutzle T, Exner TE (2009) Empirical scoring functions for advanced protein-ligand docking with PLANTS. *J Chem Inform Model* 49(1):84–96. doi:[10.1021/ci800298z](https://doi.org/10.1021/ci800298z)
53. Word JM, Lovell SC, Richardson JS, Richardson DC (1999) Asparagine and glutamine: using hydrogen atom contacts in the choice of side-chain amide orientation. *J Mol Biol* 285(4):1735–1747. doi:[10.1006/jmbi.1998.2401](https://doi.org/10.1006/jmbi.1998.2401)
54. Douguet D (2010) e-LEA3D: a computational-aided drug design web server. *Nucleic Acids Res* 38:W615–621. doi:[10.1093/nar/gkq322](https://doi.org/10.1093/nar/gkq322) (Web Server issue)
55. Wallace AC, Laskowski RA, Thornton JM (1995) LIGPLOT: a program to generate schematic diagrams of protein-ligand interactions. *Protein Eng* 8(2):127–134
56. Reynes C, Host H, Camproux AC, Laonde G, Leroux F, Mazars A, Deprez B, Fahraeus R, Villoutreix BO, Sperandio O (2010) Designing focused chemical libraries enriched in protein-protein interaction inhibitors using machine-learning methods. *PLoS Comput Biol* 6(3):e1000695. doi:[10.1371/journal.pcbi.1000695](https://doi.org/10.1371/journal.pcbi.1000695)
57. Gupta A, Bai T, Murphy V, Strike P, Anders RF, Batchelor AH (2005) Refolding, purification, and crystallization of apical membrane antigen 1 from *Plasmodium falciparum*. *Protein Expr Purif* 41(1):186–198. doi:[10.1016/j.pep.2005.01.005](https://doi.org/10.1016/j.pep.2005.01.005)
58. Zhang XD (2008) Novel analytic criteria and effective plate designs for quality control in genome-scale RNAi screens. *J Biomol Screen* 13(5):363–377. doi:[10.1177/1087057108317062](https://doi.org/10.1177/1087057108317062)
59. Cheng Y, Prusoff WH (1973) Relationship between the inhibition constant (K₁) and the concentration of inhibitor which causes 50 per cent inhibition (I₅₀) of an enzymatic reaction. *Biochem Pharmacol* 22(23):3099–3108
60. DeLean A, Munson PJ, Rodbard D (1978) Simultaneous analysis of families of sigmoidal curves: application to bioassay, radioligand assay, and physiological dose-response curves. *Am J Physiol* 235(2):E97–E102
61. Sanders MP, Barbosa AJ, Zarzycka B, Nicolaes GA, Klomp JP, de Vlieg J, Del Rio A (2012) Comparative analysis of pharmacophore screening tools. *J Chem Inform Model* 52(6):1607–1620. doi:[10.1021/ci2005274](https://doi.org/10.1021/ci2005274)
62. Vulliez-Le Normand B, Tonkin ML, Lamarque MH, Langer S, Hoos S, Roques M, Saul FA, Faber BW, Bentley GA, Boulanger MJ, Lebrun M (2012) Structural and functional insights into the malaria parasite moving junction complex. *PLoS Pathog* 8(6):e1002755. doi:[10.1371/journal.ppat.1002755](https://doi.org/10.1371/journal.ppat.1002755)
63. Krier M, Bret G, Rognan D (2006) Assessing the scaffold diversity of screening libraries. *J Chem Inform Model* 46(2):512–524. doi:[10.1021/ci050352v](https://doi.org/10.1021/ci050352v)
64. Monge A, Arrault A, Marot C, Morin-Allory L (2006) Managing, profiling and analyzing a library of 2.6 million compounds gathered from 32 chemical providers. *Mol Divers* 10(3):389–403. doi:[10.1007/s11030-006-9033-5](https://doi.org/10.1007/s11030-006-9033-5)
65. Spangenberg T, Burrows JN, Kowalczyk P, McDonald S, Wells TN, Willis P (2013) The open access malaria box: a drug discovery catalyst for neglected diseases. *PLoS One* 8(6):e62906. doi:[10.1371/journal.pone.0062906](https://doi.org/10.1371/journal.pone.0062906)
66. Sperandio O, Reynes CH, Camproux AC, Villoutreix BO (2010) Rationalizing the chemical space of protein-protein interaction inhibitors. *Drug Discov Today* 15(5–6):220–229. doi:[10.1016/j.drudis.2009.11.007](https://doi.org/10.1016/j.drudis.2009.11.007)
67. Li X, He Z, Chen L, Li Y, Li Q, Zhao S, Tao Z, Hu W, Qin L, Chen X (2011) Synergy of the antiretroviral protease inhibitor indinavir and chloroquine against malaria parasites in vitro and in vivo. *Parasitol Res* 109(6):1519–1524. doi:[10.1007/s00436-011-2427-z](https://doi.org/10.1007/s00436-011-2427-z)
68. Zhang JH, Chung TD, Oldenburg KR (1999) A simple statistical parameter for use in evaluation and validation of high throughput screening assays. *J Biomol Screen* 4(2):67–73
69. Higuero AP, Schreyer A, Bickerton GR, Pitt WR, Groom CR, Blundell TL (2009) Atomic interactions and profile of small molecules disrupting protein-protein interfaces: the TIMBAL database. *Chem Biol Drug Des* 74(5):457–467. doi:[10.1111/j.1747-0285.2009.00889.x](https://doi.org/10.1111/j.1747-0285.2009.00889.x)
70. Hamon V, Bourgeas R, Ducrot P, Theret I, Xuereb L, Basse MJ, Brunel JM, Combes S, Morelli X, Roche P (2014) 2P2I HUNTER: a tool for filtering orthosteric protein-protein interaction modulators via a dedicated support vector machine. *J R Soc Interface* 11(90):20130860. doi:[10.1098/rsif.2013.0860](https://doi.org/10.1098/rsif.2013.0860)
71. Tse C, Shoemaker AR, Adickes J, Anderson MG, Chen J, Jin S, Johnson EF, Marsh KC, Mitten MJ, Nimmer P, Roberts L, Tahir SK, Xiao Y, Yang X, Zhang H, Fesik S, Rosenberg SH, Elmore SW (2008) ABT-263: a potent and orally bioavailable Bcl-2 family inhibitor. *Cancer Res* 68(9):3421–3428. doi:[10.1158/0008-5472.CAN-07-5836](https://doi.org/10.1158/0008-5472.CAN-07-5836)